Journal of Sol-Gel Science and Technology 8, 117–123 (1997)

Structural Models of Dense Gels

JULIAN RODRÍGUEZ-ORTEGA AND LUIS ESQUIVIAS
Departamento de Física de la Materia Condensada, Facultad de Ciencias, Universidad de Cádiz, Apartado 40, Puerto Real, 11510 Cádiz, Spain

Abstract. The structural models of gels typically reported concentrate either on the "solid space" or the "pore space" of the system. The models described in this paper present a connection between grain and pore spaces, applicable to dense gels with uniform particulate microstructure. The gel structure is depicted as a hierarchy at several levels by means of models built up using the Monte-Carlo technique, on the basis of random close packing (RCP) premises. The pore volume distributions are calculated from the largest sphere radius inscribed within the interstices. These distributions are compared to the pore volume distributions of various RCP classic models and to the pore volume distributions of a series of xerogels measured by means of the Brunauer-Emmett-Teller method. Data on the pore volumes associated with different hierarchical levels (e.g., micro-, meso-, or macropores), the local density of the i-th aggregation level and packing of the successive levels are obtained.

Keywords: structure, silica gels, RCP, pore volume

1. Introduction

The structural[1] study of dry gels is mainly carried out from adsorption methods, like Brunauer-Emmet-Teller (BET) and Hg intrusion porosimetry, completed with Small Angle Neutron or X-ray Scattering (SANS or SAXS) and Electron Microscopy (EM). The analysis of these data is marked by the fact that the pore size distribution of gels is spread over a few orders of magnitude and, accordingly, the densities strongly depend on the experimental resolution. This is important when modeling is intended because the first condition to accomplish by any geometrical model is matching the mass distribution. Nevertheless, some gels have particular structural characteristics by their special preparation conditions that, with an adequate strategy, can facilitate their study. Thus, in the case of sonogels, the solventless processing and the cavitation phenomenon, responsible for the alkoxide-water mixture homogenization, yield a very narrow distribution of pores. The same is true when Drying Control Chemical Additives (DCCA) or a combination of both external agents is used [1, 2]. In this case, the SAXS intensity curves indicate a quasi monodisperse distribution of particulate scatterers. These facts immediately suggest to implement a macroscopic 3-D image of these gels by means of a "solid space" based geometrical model such as a collection of packed spherical particles.

In many cases, the mass distribution and EM observations of gels, although they cannot be quantitatively interpreted, suggest some kind of hierarchic arrangement. As a consequence, the fractal geometry was in fashion recently, but most of gels, except the very light ones, do not fulfill the autosimilarity condition over one order of magnitude at least [3]. However, this does not represent any drawback for the dense gels. Indeed, a fractal description only requires that a part is similar to the whole but does not give any information on the geometrical arrangement of particles nor topology. On the contrary, the texture of dense gels has certain features, as it is shown in this paper, that permit an approach from simple adsorption data.

2. Description of the Method

The strategy to build the models is to extract "pore space" features from a model based on the "solid space" and compare it to the experimental measurements [4]. Micro-, meso-, and macropores are also

classified according to the particle arrangement. Type I pores are those interstices between four contacting particles. Pores of type II are holes between not contacting particles which are not large enough to contain at least one particle, otherwise, it is type III. In this sense, the pore size distributions of Random Close Packing (RCP) models are adequate to account for dense gel structures because they have no type I pores. On the other hand, although EM shows that dense gel have type I pores, they do not contribute appreciably in the BET obtained porous volume distribution of dense gels. Thus, the structure of dense gels can be approached by a distribution of particles allowing micro- and mesopores between them.

Zarzycki [4, 5] initiated this approach comparing pore size distribution of gels with that of the random close-packed hard sphere model studied by Bernal and Mason [6, 7], Scott [8] and Finney [9]. The texture of gels is generated on the basis of two critical magnitudes such as the *compactness of the packing*, $C =$ (volume spheres)/(total volume) and the average coordination number, $\overline{\text{CN}}$. They are almost linearly related by $\overline{\text{CN}} \approx 12.7C$ [10, 11], having a maximum in $\overline{\text{CN}} \approx 8$, and depend on the definition of the *closeness of the contact*. This is given by the range of center-to-center to diameter ratio (L/d) adopted to identify two spheres as being coordinated. The pore size distribution is given by the volume of the largest sphere radii inscribed in the interstices [12]. This constitute rather a local gauge of the channels which are formed from a succesion of interstitial sites and which may be linked by constrained neckes [13]. The series is expressed as a function of a reduced variable $K (K = r/R, r$ being the pore radius and R the particle radius). In this way, the results could be extrapolated to whatever particle size.

These RCP structures, are "ideal". Concerning their applicability to depict the texture of gels, their failing could be a lack of versatility and dynamism to adapt the characteristics of each particular gel. In this respect, formerly applied to describe the atomic structure of metallic glasses, a network created from randomly distributed nucleation spots harmonizes better with the nature of the gelling kinetics and gel consolidation. The alternative we present here is dynamic in the sense that we are able to fit the model to the real conditions of each particular case. Thus, the models are not purely geometric but they were submitted to different process of relaxation and "hollowing out". Thereby, we have created a catalog of pore size distributions and compared them to that of a series of gels prepared in different conditions to choose the more appropriate model.

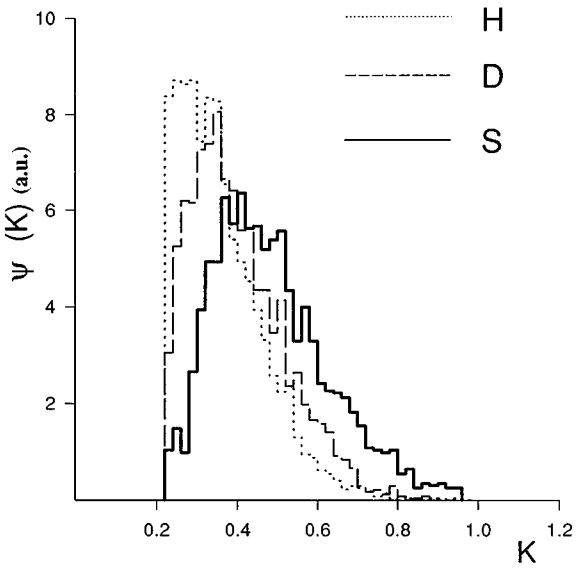

Figure 1. Interstice distribution functions for H, D and S models. $K = r/R$ where r is the radius of the largest inscribed sphere and R the particle radius.

The catalog was generated from three basic spherical models, H, D and S of diameters, $D \sim 20$ R. Table 1 accounts for the closeness of contact conditions and resulting compactness of each case. In Fig. 1 are represented their pore size distributions, $p(K)$. The S model, as in Scott's loose model [8], should be mainly formed by octaedra, slightly distorted, because the maximum of the distribution is near $K = K_{\max} = 0.414$, which corresponds to octahedral sites. The D model has the maximum population of pores for $K_{\max} = 0.34$. This is a consequence of allowing interpenetration or deformation of the spheres. The distribution is intermediate between the Finney's [9] and Scott's [8] models. The H model allows 10% of radial deformation giving rise to a model with the maximum of the distribution $K_{\max} = 0.25$, not far from that corresponding to the tetrahedral sites ($K_T = 0.225$). Finney's model has $K_{\max}$ at 0.3, although it is a little more compact, the distribution ranging from 0.225 to 0.8.

2.1. Increasing the Porosity and Relaxing the System

The models are assisted to converge toward a particular structure introducing random voids into the structure [14] and relaxing the network applying the Lennard-Jones potential [15]. The distribution of minimum energy is found by a Monte Carlo algorithm.

The models are identified according the following nomenclature: X Py Lz

X indicates the type of model: H, D, S.
y is the percentage of added porosity.
$z = 10\sigma$ parameter Lennard-Jones potential, i.e., L8 means $\sigma = 0.8$. LJ indicates a non-relaxed model.

2.2. *Examining the Experimental Distributions*

The shape of the distribution function can shed light on the nature of the hierarchical structure, if it exists, of the arrangement. Let us consider an ideal model consisting of an assembly of close packed spheres of radius R_{i+1}. These spheres are formed, as well, by a similar arrangement of smaller spheres of R_i radius, q_{i+1} being the radius ratio, $q_{i+1} = R_{i+1}/R_i$. These spheres could be also formed by random close packed spheres of $R_{i-1} = R_i/q_i$ radius. The pore volume distribution of such a structure is presented in Fig. 2. This has to be compared with Frost's distribution volume derivative $\psi(K) = K^2 p(K)$ traced as a function of log K. K at the i-th level, K^i, is related to the pore size, r^i, and elementary particle size, R_0, by the relationship

$$K^i = \frac{r^i}{R_i} = \frac{r^i}{\prod_1^i q_i R_0} \tag{1}$$

with $\frac{r^0_{\max}}{r^0_t} = \frac{K^0_{\max}}{K^0_t} = a$. Therefore, from Equations (1),

$$K^i_{\max} = \frac{1}{\prod_1^i q_i a} \frac{r^i_{\max}}{r^0_t} K^0_{\max} \tag{2}$$

A kinetic study of the structure during gelation by SAXS [16] informs that there are two characteristics correlation lengths from where a model of statistics balls can be inferred. These tangles compact during aging giving rise, after drying, to aggregates (of a few tenths of Å) of nearly monosized spheroid particles

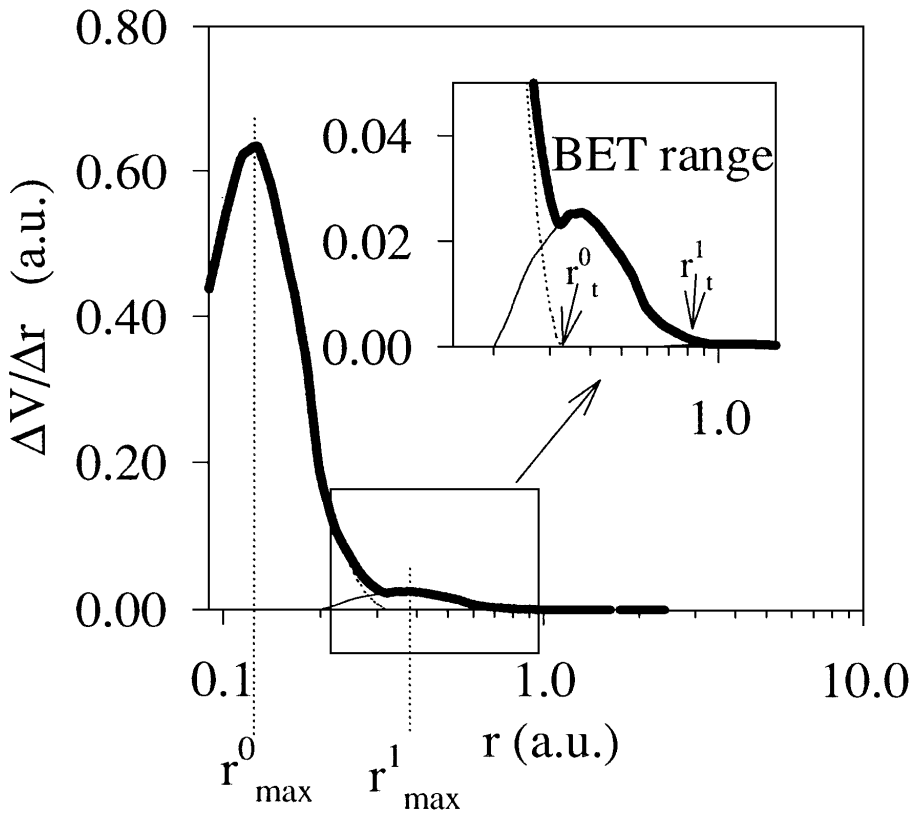

Figure 2. Pore volume distribution outline of an ideal structure formed by successive packing of spherical particles built of smaller particles random close packed.

[17, 18]. In the case of pure silica gels the size and density of these particles have been estimated to be $r \sim 1.1$ nm and $2.1\ \mathrm{g \cdot cm^{-3}}$ from the analysis of wide angle X-ray diffraction data. Unfortunately, the actual resolution threshold of a BET experiment is far from resolving the pore in aggregates of such elementary particles. We can only tell the upper tail of this distribution, $r_t^0 = K_t^0 R_0$, overlapped with the smallest pores of the first level distribution. We assume that those aggregates present only pores of types I and II (packing fraction between 0.6 and 0.7) [19].

We admit for the analysis values of a and $K^0_{\max}$ that of very close networks such as the Bernal and Finney's distribution, for example, with $a = \frac{3}{8}$ and $K^0_{\max} = 0.3$. We take this model just as a standard Anyway, we estimate that other plausible hypotheses would not give a deviation higher than 10%.

Thus, for $i = 1$,

$$K^1_{\max} \cong \frac{0.8}{q_1} \frac{r^1_{\max}}{r^0_t} \approx 0.8 \frac{r^1_{\max}}{r^1_t} \tag{3}$$

with $q_1 = \frac{r^1_t}{r^0_t}$.

Actually, in the next analysis we consider the gel structure formed by a RCP network of these clusters. At this point it is worth to remind that the $p(K)$ functions provide a quantitative way of evaluating pore-size distribution without implying necessarily spherical pores.

We use the calculated value $K^1_{\max}$ as a criterion to choose the more appropriate model from our catalog.

From the mere observation of the experimental distribution it is possible to assess whether there is some kind of hierarchic arrangement. Effectively, if the distribution range in the log scale is smaller than random-close packed spheres ($\log 0.8 - \log 0.22 = 0.56$) in the log K scale, it should be considered a multimodal distribution of independent particles because the smaller particles are located in the interstices of the larger ones. If the distribution width is larger than the loosest model distribution ($\log 1 - \log 0.22 = 0.65$), the possibility of a hierarchic structure of interpenetrating agglomerates ($q_i < 3$) has to be contemplated Fig. 3. In this case, $K^2_{\max}$ could be also estimated according to the expression (2)

$$K^2_{\max} \cong \frac{a}{q_1} \frac{r^2_{\max}}{r^0_t} \cong 0.8 \frac{r^2_{\max}}{r^2_t} \tag{4}$$

where $q_1 q_2 = \frac{r^2_t}{r^0_t}$.

3. Application of the Models

We have tested our models with some SiO_2 gels prepared by conventional mixing of tetraethylortosilicate (TEOS), water (pH = 3, HNO_3) 4[H_2O]/[TEOS] and formamide (FOR) as an additive (7[FOR]/[TEOS]). The label used to refer these samples is **E** to differentiate them from other samples presented here. The gels were heat-treated at different temperatures for variable periods of time. The heat-treatment is also indicated in the label. Thus, $\mathbf{E_{cd}}$, means an **E** type gel treated at **c** $\times$ 100°C for **d** hours. Their pore distributions are in Fig. 4.

From the examination of the volume distribution of the gel heat-treated at 400°C for 5 hr (E45), we estimate $r^1_{\max}/r^0_t \cong 1.0$ and $r^1_t/r^0_t = 3.0$. The group of possible models should have $K^1_{\max}$ near 0.27 among those, the HP0L9 gives the best fit. The aggregates average size is $R_1 = \frac{11.7}{0.28} = 42$ Å, formed by elementary particles of 14 Å. In Table 2 are the calculated structural parameters for the distributions of Fig. 4.

These calculations for an estimated value of $K^1_{\max}$ for the E95 and E105 give 0.32 and 0.28, respectively. The application of DP0L10 and DP0L9 models, respectively, result in sound fittings.

If we know the whole volume enclosed by the aggregates of elementary particles, the density of the i-level can be calculated as

$$\rho_i = \left(V_i + \frac{1}{\rho_s} \right)^{-1}$$

where ρ_s is the skeleton density and V_i is the pore specific volume at the i-level (analytically calculated). However, a part of that volume is inaccessible to N_2. For this reason the relative packing fractions, $C_i = \frac{\rho_{i+1}}{\rho_i}$, are overvalued because the densities are considering that only the measured pore volume exists. Thus, the compactness of these agglomerates increases and, consequently, the measured micropore volume approaches the actual value while the heat-treatment temperature increases. Figure 4 includes a schematic representation of the texture transformation, sintering first affecting the structure on the finest scale, as it has to be expected. The representation of the partially sintered samples, such as that heat-treated at 1000°C, it has to be understood as, in areas where pores exist (type I or II), it is produced by the depicted geometry; that is, close packed particles of R_1 average radius. The relative amount of gel presenting this structure

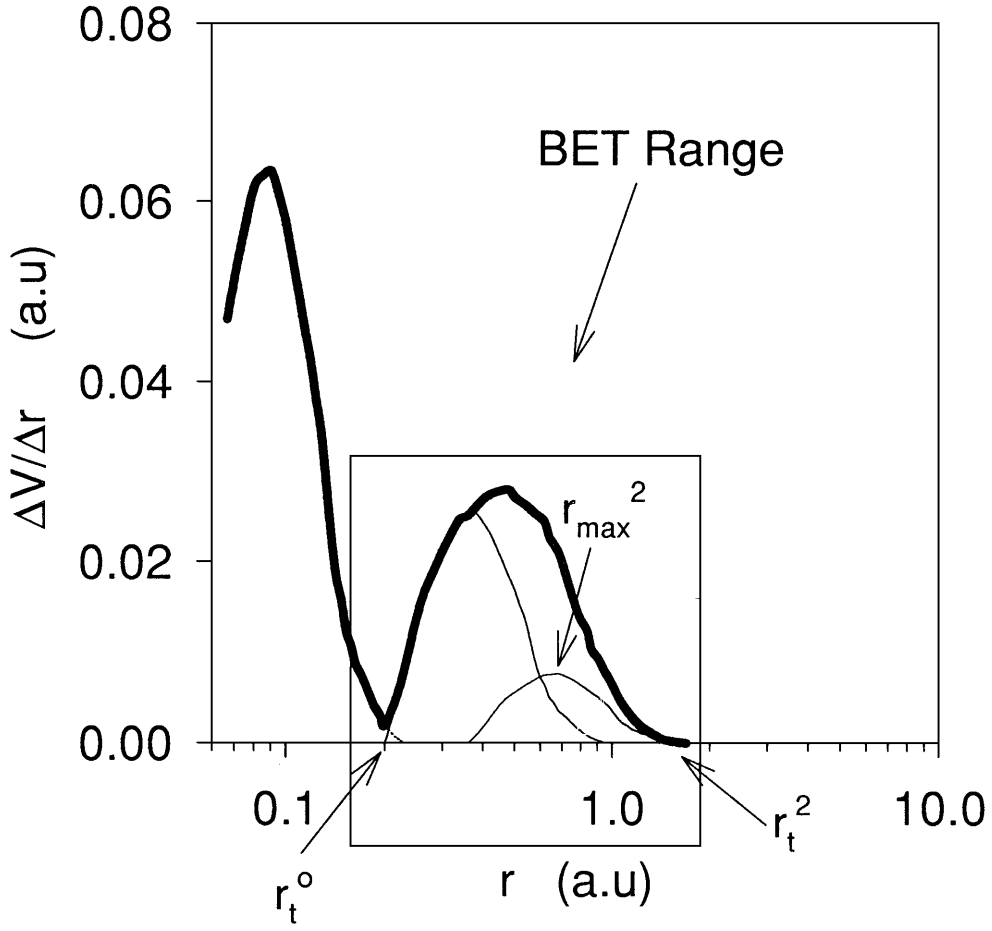

Figure 3. Ibid. Fig. 2. In this case the third level is formed by interpenetrating particles.

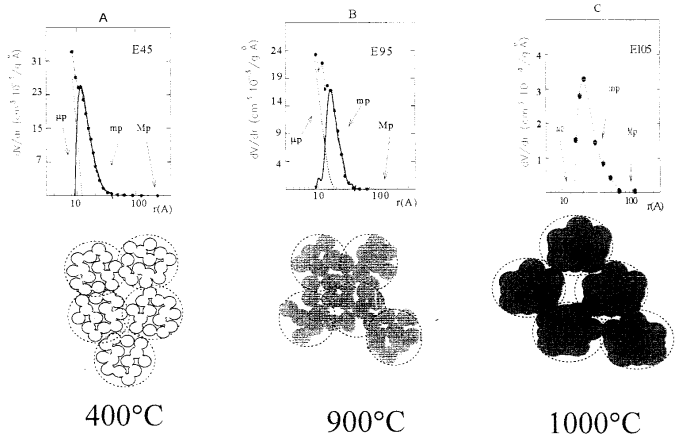

Figure 4. Interpretation of pore size distributions of SiO_2 dry gels prepared with formamide as DCCA. (Mp, macropores, mp, mesopores, μp, micropores). The mesopore fraction was fitted with the models indicated in Table 2. Below there is a schematic representation of the texture transformation. This has to be understood as, in areas where mesoporosity exists, it is produced by the depicted geometry, that is, close packed particles of R_1 average radius.

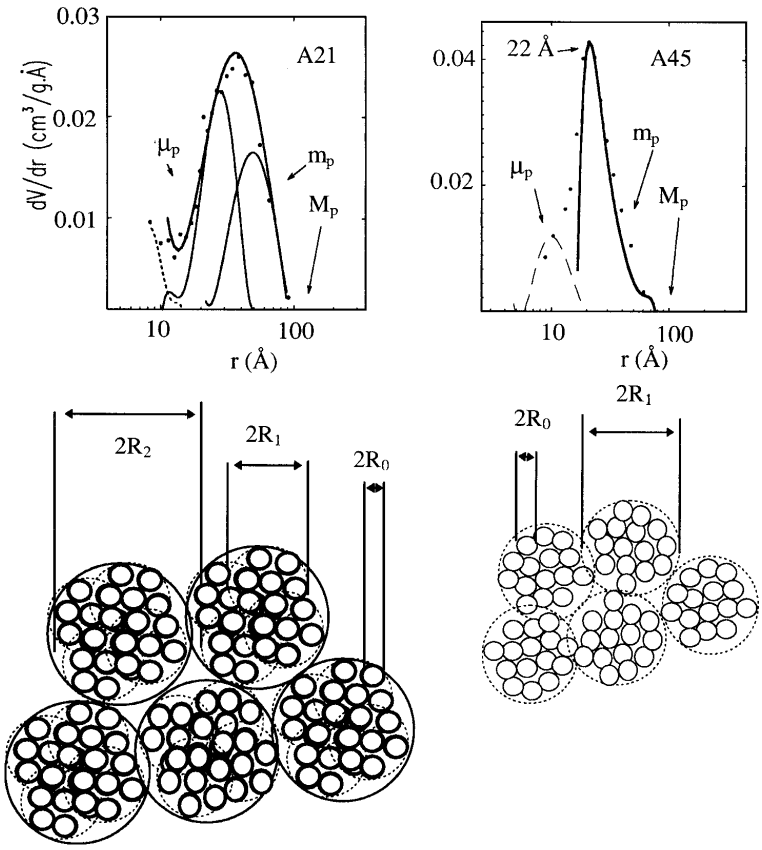

Figure 5. Interpretation of pore size distribution of SiO_2 sono-xerogels. (Mp, macropores, mp, mesopores, μp, micropores). Below there is a schematic representation of the texture transformation. The mp fraction was fitted convoluting the distribution of two selected model (see text). These second order aggregates compact when formamide evolves (A45 sample).

is given by the ratio between the real mesopore volume (measured as the area beneath the experimental curve) and the model pore volume. For exemple, in the case of the sample treated at 1000°C, this quotient is $0.01/0.32 \cong 3\%$.

We have also described with our models the structure of sono-xerogels. The ultrasonic energy dose was 0.3 KJ/cm^3. These samples were labeled **A**.

The case of a sample heated at 200°C for 1 hr (A21) is a positive example where two mesopore distributions should be considered. An approximate value of $K^2_{\max}$ is $0.8\frac{50}{100} = 0.40$ with $q_1 q_2 = \frac{100}{16} = 6.3$. In the same way, $K^1_{\max} \approx \frac{0.8}{q_1} \cdot \frac{30}{16} \approx 0.5$, supposing $q_1 \cong 3$. With this figures as a guide, the possible models are tested, keeping in mind that q_2 should be less than 3. The combination of the models SP18LJ for the first level and DP18L12 for the second one fits the experimental volume distribution (Fig. 5). As the formamide and other organics have not yet been eliminated, the network is formed by very loose aggregates of more than 100 Å. These aggregates are formed by smaller interpenetrating clusters of 70 Å radius formed by elementary particles of ∼20 Å. 60% of its specific pore volume, $V_T = 1.02\,\text{cm}^3 \cdot \text{g}^{-1}$ correspond to macropores and 39% to mesopores. The model HP0L9 fits the distribution of this gel heated up to 400°C for 5 hr. The formamide has evolved and the aggregates compact (Fig. 5) up to 88 Å radius. The elementary particle radius is still 20 Å. 77% of its specific pore volume ($0.69\ \text{cm}^3 \cdot \text{g}^{-1}$) are mesopores and 20% macropores.

4. Conclusions

The structure of some xerogels is depicted as successive levels of hierarchic random close packed networks. A catalog of the average estimates of the pores internal volume ($\Psi(K)$ functions) of models created from

randomly distributed particles helps to describe it. The value of K at which $\Psi(K)$ presents its maximum gives a criterion to choose the more adequate model. Gels presenting a large pore distribution can be described as hierarchic structure of interpenetrating agglomerates.

Acknowledgment

Authors thanks the Junta de Andalucía for financial support (Exp. #6015).

Note

1. Along this paper, we employ the term structure to refer the or mutual disposition of both phases or texture.

References

1. N. de la Rosa-Fox, L. Esquivias, and J. Zarzycki, J. Material. Sci. Let. **10**, 1237 (1991).
2. E. Blanco, M. Ramírez del Solar, L. Esquivias, and A.F. Craievich, J. Non-Cryst. Solids **147**&**148**, 296 (1992).
3. J. Zarzycki, J. Non-Cryst. Solids **121** (1992)
4. J. Zarzycki, in *Chemical Processing of Advanced Materials* edited by L.L. Hench and J.K. West (John Wiley & Sons, Inc. New York, 1992), p. 84.
5. J. Zarzycki, J. Non-Cryst. Solids **147**&**148**, 176 (1992).
6. J.D. Bernal and J. Mason, Nature **188**, 910 (1960).
7. J.D. Bernal, *Proc. R. Soc.* (1964), **280A**, 299.
8. G.D. Scott, Nature **188**, 908 (1960).
9. J.L. Finney, *Proc. R. Soc.* (London) **A319**, 479, (1970).
10. T. Ichikawa, Phys. Stat. Sol. (a) **29**, 293 (1975).
11. J. Blétry and Z. Naturf (a) **32**, 445 (1977).
12. H. Frost, ONR Technical Report No. 6 (Division of Applied Sciences, Harvard Univ., Cambridge, MA, 1978).
13. See Fig. 8 in ref. [5].
14. J.D. Bernal and S.V: King, Discuss. Faraday Soc. **43**, 60 (1967).
15. J.L. Finney and J. Wallace, J. Non-Cryst. Solids **43**, 165 (1981).
16. M. Ramírez del Solar, L. Esquivias, A.F. Craievich, and J. Zarzycki, J. Non-Cryst. Solids **147**&**148**, 296 (1992).
17. N. de la Rosa-Fox, L. Esquivias, A. Craievich, and J. Zarzycki, J. Non-Cryst.Solids **121**, 211 (1990).
18. M.C. Barrera-Solano, N. de la Rosa-Fox, and L. Esquivias, J. Non-Cryst. Solids **147**&**148**, 194 (1992).
19. N. de la Rosa-Fox, E. Blanco, and L. Esquivias, *Proc. VIII International Conference on the Physiscs of Non Crystalline Solids* (Turku, Finland 1995), J. Non-Cryst. Solids (in press).